

## Collective effects in artificial two-dimensional lattices of ferromagnetic nanoparticles

This article has been downloaded from IOPscience. Please scroll down to see the full text article.

2000 Phys.-Usp. 43 288

(<http://iopscience.iop.org/1063-7869/43/3/A06>)

View [the table of contents for this issue](#), or go to the [journal homepage](#) for more

Download details:

IP Address: 128.59.62.83

The article was downloaded on 26/07/2012 at 13:06

Please note that [terms and conditions apply](#).

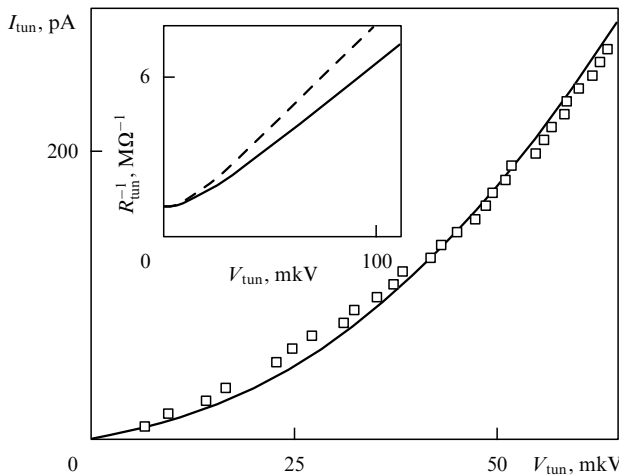


**Figure 4.** Comparison of measured and computed [Eqn (5)] current–voltage characteristics in the  $R_{\text{tun}}$  maximum at  $\nu \approx 1$  for sample B;  $T = 60$  mK,  $B = 13$  T. The inset shows the fitting curve for  $V_{\text{tun}}, R_{\text{tun}}^{-1}$  before (dashed line) and after (solid line) computation of the first Fourier harmonic.

the results of earlier experiments [7]. The current–voltage characteristics for the filling factor  $\nu = 2/3$  were close to linear ones even at  $eV_{\text{tun}} > k_B T$ , although the linear range shrank with increasing temperature.

To conclude, we have confirmed the existence of a linear-in-energy pseudogap over a wide range of filling factors at  $\nu < 1$  (outside the tunneling-resistance peaks at  $\nu = 1/3$  and  $\nu = 2/3$ ) and demonstrated that the linear energy dependence also holds for a double-humped structure near  $\nu = 1$ . It follows from the analysis of current–voltage characteristics that the coefficient  $\alpha$  peaks at  $\nu = 1$ . By comparing the positions of the peaks of the real current component near  $\nu = 1$  and metal–insulator transition points in samples of similar quality [23], the filling factors corresponding to the peaks were found to coincide with the filling factors at the transition points. In principle, the available theoretical models allow one to describe a decrease of the coefficient  $\alpha$  associated with a deviation of the filling factor from  $\nu = 1$ .

According to Refs [17, 18], tunneling into the metallic phase leads to the development of a pseudogap related to the finite time of charge dissipation in the plane. The higher the conductance in the plane, the narrower the gap. The shape of the gap in the metallic phase is given by the expression

$$D(\varepsilon) = D_{\text{th}} \exp\left(-\ln^2 \frac{e^4}{\alpha^2 K |\varepsilon - \varepsilon_F|}\right). \quad (6)$$

Here,  $D_{\text{th}}$  is the thermodynamic density of states and  $K$  is the diffusion coefficient [18, 24]. According to [24], dependence (6) in the energy interval  $|\varepsilon - \varepsilon_F| < U_c = e^2/\alpha\xi$  ( $\xi$  is the mean dimension of the conducting cluster) must be replaced by  $\alpha|\varepsilon - \varepsilon_F|$ , where  $\alpha = D(\varepsilon_F + U_c)/U_c$ . It has been shown experimentally that the coefficient  $\alpha$  increases as  $\nu \rightarrow 1$ , because the correlation length  $\xi$  decreases with penetration deeper into the dielectric phase.

This work was supported by the Russian Foundation for Basic Research (project 97-02-16829); the Program ‘‘Physics of Solid-State Nanostructures’’ (project 97-1024) and Program ‘‘Statistical Physics’’ of the Russian Ministry of Science and Technology; and Program ‘‘Physics of Nanostructured Solids’’ (Deutsche Forschungsgemeinschaft, Germany).

## References

1. Chang A M, Pfeiffer L N, West K W *Phys. Rev. Lett.* **77** 2538 (1996)
2. Grayson M et al. *Phys. Rev. Lett.* **80** 1062 (1998)
3. Shashkin A A et al. *Pis'ma Zh. Eksp. Teor. Fiz.* **69** 561 (1999) [*JETP Lett.* **69** 603 (1999)]
4. Ashoori R C et al. *Phys. Rev. Lett.* **64** 681 (1990)
5. Ashoori R C et al. *Phys. Rev. B* **48** 4616 (1993)
6. Eisenstein J P, Pfeiffer L N, West K W *Phys. Rev. Lett.* **69** 3804 (1992); **74** 1419 (1995)
7. Chan H B et al. *Phys. Rev. Lett.* **79** 2867 (1997)
8. Brown K M et al. *Phys. Rev. B* **50** 15465 (1994)
9. Dolgoplov V T et al. *Phys. Rev. B* **51** 7958 (1995)
10. Chan H B et al., cond-mat/9905371
11. Eisenstein J P, Pfeiffer L N, West K W *Phys. Rev. B* **50** 1760 (1994)
12. Dolgoplov V T et al. *Phys. Rev. Lett.* **79** 729 (1997)
13. Altshuler B L, Aronov A G, Lee P A *Phys. Rev. Lett.* **44** 1288 (1980)
14. Efros A L, Shklovskii B I, in *Electron–Electron Interaction in Disordered Systems* (Eds A L Efros, M Pollak) (Amsterdam: North-Holland, 1985)
15. Efros A L *Phys. Rev. Lett.* **68** 2208 (1992)
16. Hatsugai Y, Bares P -A, Wen X G *Phys. Rev. Lett.* **71** 424 (1993)
17. He S, Platzman P M, Halperin B I *Phys. Rev. Lett.* **71** 777 (1993)
18. Levitov L S, Shytov A V *Pis'ma Zh. Eksp. Teor. Fiz.* **66** 200 (1997) [*JETP Lett.* **66** 214 (1997)]
19. Johansson P, Kinaret J M *Phys. Rev. Lett.* **71** 1435 (1993)
20. Aleiner I L, Baranger H U, Glazman L I *Phys. Rev. Lett.* **74** 3435 (1995)
21. Yang S -R E, MacDonald A H *Phys. Rev. Lett.* **70** 4119 (1993)
22. Dolgoplov V T et al. *Phys. Low-Dim. Struct.* (6) 1 (1996)
23. Shashkin A A et al. *Phys. Rev. Lett.* **73** 3141 (1994)
24. Polyakov D G, Samokhin K V *Phys. Rev. Lett.* **80** 1509 (1998)

PACS numbers: 75.60.-d, 75.70.-k  
DOI: 10.1070/PU2000v043n03ABEH000700

## Collective effects in artificial two-dimensional lattices of ferromagnetic nanoparticles

S A Gusev, Yu N Nozdrin, M V Sapozhnikov, A A Fraerman

Many studies of zero-dimensional nanostructures are focused on the creation and investigation of ferromagnetic nanoparticles. On the one hand, interest in these particles is due to the possibility of their practical application, in the first place for the development of recording media that can ensure super-high (over  $10^{10}$  bit  $\text{cm}^{-2}$ ) data storage densities [1]. On the other hand, studies of ferromagnetic nanoparticles bring about new knowledge of the properties of magnetic materials at supersmall scales.

We believe that the collective behavior of ferromagnetic nanoparticles during their interaction is one of the most interesting aspects of the problem in question. Stray fields induced by individual particles constitute the fundamental cause of this interaction. In the case of a single-domain particle, the major contribution comes from dipole interaction. Elucidation of this mechanism has important practical implications, because it may be useful for the assessment of data density limits.

Creation of systems of interacting ferromagnetic nanoparticles opens good prospects for the control of magnetic properties. Indeed, if we mentally substitute single-domain supermagnetic particles for magnetic atoms, it would be possible, by virtue of their dipole interaction, to effect a

phase transition from a disordered (superparamagnetic) to an ordered (ferromagnetic) state.

The critical temperature of this phase transition depends on the dipole interaction energy of the order of  $T_c \sim M^2 V^2 / R^3$ , where  $M$  is the saturation magnetic moment,  $V$  is the particle volume, and  $R$  is the distance between particles. Owing to the anisotropic and long-range character of dipole interactions, the type of long-range order strongly depends on the lattice symmetry [2]. By changing the lattice symmetry and interparticle distance, it is possible to control both the type of long-range order and critical temperature of a magnet.

The existence of supermagnetism in two-dimensional lattices of ferromagnetic nanoparticles was first postulated in Ref. [3]. Ref. [4] reports the results of experiments which appear to confirm such a transition. However, details of this process remain to be clarified. We therefore decided to undertake a theoretical and experimental study of dipole interactions in ordered lattices of ferromagnetic nanoparticles. Our findings are presented below.

Two-dimensional lattices of ferromagnetic nanoparticles were produced from permalloy ( $\text{Ni}_3\text{Fe}$ ) films by means of electron-beam lithography. The films were deposited onto a substrate by laser-assisted evaporation. The electronic resists were exposed and the resulting lattice morphology was examined in a JEM-2000EX electron microscope. The lattice patterns were formed using a film of  $\text{C}_{60}$  fullerene as the negative electronic resist and a Ti film as the conducting layer. The fullerene layer was applied by thermal evaporation, and the Ti film, by laser sputtering.

After treatment with an electron beam, the sample was rinsed in toluene to obtain a mask of a desired configuration. Plasmachemical etching of Ti layers was performed in an atmosphere of  $\text{CF}_2\text{Cl}_2$ , the resulting pattern was transferred onto the film by ionic etching in an Ar atmosphere. This approach made it possible to prepare two-dimensional lattices composed of cylindrical particles with a diameter from 15 to 100 nm and a height determined by the primary film thickness (10–50 nm). The particles' lateral dimensions depended on the time of resist exposure to the electron beam and the duration of plasmachemical and ion etching.

Figure 1a shows an electron micrograph of a part of a system of permalloy nanoparticles 40–50 nm in diameter and 45 nm in height which form a lattice having a rectangular unit cell  $90 \times 180$  nm in size. The number of particles in the lattice is on the order of  $10^5$ . Figure 1b presents a general view of the sample with a distinct large-scale moiré pattern resulting from the inconsistency between the raster periodicity of the

electron microscope and the lattice period. This pattern suggests regularity of the lattice.

A disadvantage of the above method for the creation of two-dimensional lattices is the small permissible size of the sample, which cannot exceed  $100 \mu\text{m}$ . The possibility of multiplication is limited by the time necessary to form the pattern: it takes about two hours to create a  $100 \times 100 \mu\text{m}^2$  lattice with an electron microscope. This limitation causes serious methodological difficulties which impede experimental studies of the magnetic properties of lattices obtained by the above technique.

In the present study, as in Refs [5, 6], the magnetic properties of lattices formed of permalloy nanoparticles were investigated using a system of two semiconductor (InSb) Hall sensors with a common potential and independent current contacts. The working area of  $10\text{-}\mu\text{m}$ -thick sensors was  $50 \times 100 \mu\text{m}^2$ . The system to be examined was formed in the working area of one sensor. Its location on the Hall sensor is shown in Fig. 1b.

Assuming that permalloy consists of 40-nm single-domain particles (see, for example, [7]) involved in magnetodipole interactions, it follows from the system's symmetry that the easy magnetization axis lies in the plane of the sample and is parallel to the smaller lattice vector. In order to detect this anisotropy, we obtained magnetization curves at different orientations of the external field with respect to the lattice axes. The direction of the external magnetic field was determined by two angles,  $\theta$  and  $\varphi$ , where  $\theta$  is the angle counted from the normal to the sample (axis  $z$ ) and  $\varphi$  is the azimuthal angle taken from the axis parallel to the chain of particles (axis  $x$ ).

We made measurements for the following three orientations of the external magnetic fields: (1)  $\theta = \pi/4$ ,  $\varphi = 0$ ; (2)  $\theta = \pi/4$ ,  $\varphi = \pi/2$ ; and (3)  $\theta = 0$ . The resulting magnetization curves for  $T = 4.2$  K are presented in Figs 2 and 3 (thick line). The dependence of the magnetization curves on the field orientation relative to the lattice axes cannot be accounted for by the properties of individual particles and actually ensues from their collective behavior. Surprisingly, we observed a residual magnetic moment after magnetization for the orientations of the external magnetic field (2) and (3). In an earlier work [8], we suggested that this residual magnetization may be related to the formation of heterogeneous states (solitons) in the system under consideration, which resembles a quasi-uni-dimensional one.

The results of numerical calculations indicate that perpendicular anisotropy in particles of which the lattice is composed is indispensable for the existence of residual

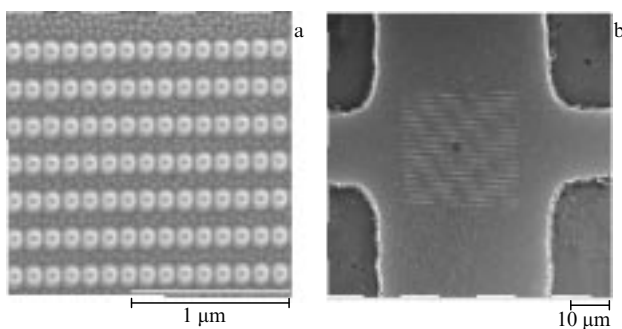


**Figure 1.** Electron micrograph of a sample: (a) fragment of a regular lattice of ferromagnetic nanoparticles overlying an uneven substrate; (b) sample located on the sensor.

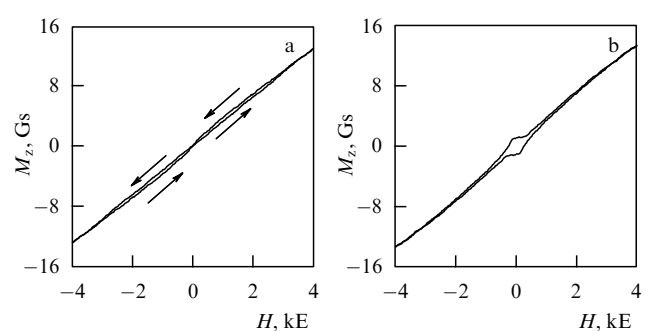


**Figure 2.** Magnetization curves of a sample for different directions of the external magnetic field: (a)  $\theta = \pi/4$ ,  $\varphi = 0$ ; (b)  $\theta = \pi/4$ ,  $\varphi = \pi/2$ .  $T = 4.2$  K.

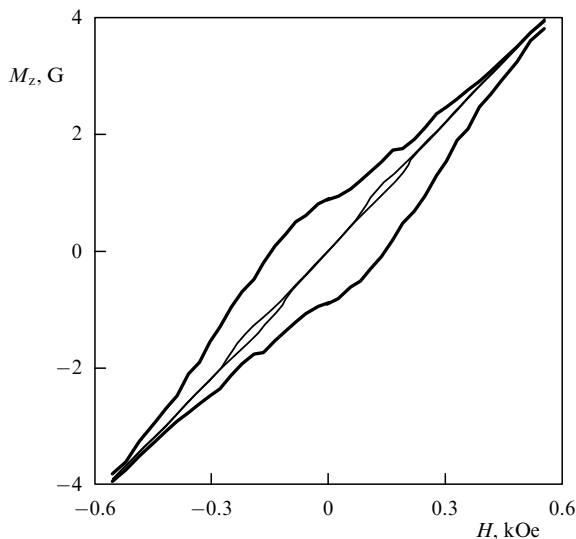


**Figure 3.** Temperature dependence of the hysteresis loop in an external magnetic field perpendicular to the sample ( $\theta = 0$ ): thick line,  $T = 4.2$  K, thin line,  $T = 77$  K.

magnetization. We changed the particle shape without altering the lattice parameters (the particle height was reduced to 25 nm while their diameter was increased to 80 nm). Thereby, the single-particle anisotropy was significantly modified. This, however, failed to cause a qualitative change in the shape of the magnetization curves. This finding questions the validity of the earlier ‘soliton’ hypothesis of hysteresis left by lattice magnetization in the hard direction. It can be speculated that the effect observed in our study was related to the inhomogeneous distribution of magnetization in the particles constituting the lattice.

Micromagnetic calculations have demonstrated [9] that, with the tabulated values of the exchange interaction constant ( $J \approx 0.55 \times 10^6$  erg cm), magnetic moment ( $M_s \sim 10^3$  G), and anisotropy constant ( $K \sim 10^3$  erg cm $^{-3}$ ), the isolated permalloy particles 20–40 nm in diameter and 20–40 nm in height form vortex patterns of magnetization. The critical radius of transition to the homogeneous state is 10 nm. It is therefore possible to postulate the following scenario of the magnetization process. The magnetization distribution in the particles is homogeneous when the external magnetic field is oriented parallel to the rows. In this case, magnetic moments of individual particles are also parallel and their interaction energy is minimum. The reduced interaction energy is also beneficial for the homogeneous distribution of magnetization in a zero field.

The interaction energy is maximum when magnetizing occurs in fields perpendicular to the particle chains. The decrease of this energy, as well as of the self-energy of an individual particle is achieved by ‘folding’ the magnetization distribution into a vortex. This situation is reminiscent of what was observed in the experiment, bearing in mind that the vortex distribution must have a finite value of the  $z$  component of the magnetic moment. The presence of a residual  $z$  component is related to the requirement of finiteness of the exchange energy in the center of the vortex and was discussed in Ref. [10]. This hypothesis needs to be verified by an additional calculation of the magnetization distribution in particles taking into account interactions between them.

Hysteresis loops in the system under study have important peculiarities when the magnetic field is aligned with the particle rows (Fig. 4). In this case, even the very fact of registration of a signal seems quite unexpected. Indeed, Hall magnetometry detects the  $z$  component of field  $B$  generated by the sample averaged over the area. The appearance of the normal component when the field is applied in the sample plane may be due either to the asymmetric location of the lattice relative to the sensor or to the fact that the sensor is not ideal, e.g., is wedge-shaped. We observed the hysteresis loop shown in Fig. 4 in samples with a unit cell whose sides had the ratio 1:2. A peculiar feature of the magnetization process in this observation was the transition from one branch of the hysteresis loop to another resulting from a change in the sign of the time derivative of the external field.

In the case of an antiferromagnetic interaction between chains, which decreases according to a power law [11], and of their infinite number, the magnetization curve should be expected to show fractal behavior. Such a situation holds in the analysis of the relationship between the density of a one-dimensional lattice gas characterized by the long-range antiferromagnetic interaction and the chemical potential [12].

An essential characteristic of the problem of the magnetization reversal of the chains is the coercivity of the chains. Direct simulation of the magnetization reversal of a system of a chain of dipoles has demonstrated a stepwise structure of the hysteresis edge, with the height of each step being equal to the magnetic moment of an individual chain and the length determined by the type of interaction between the chains (Fig. 5). Their magnetization reversal in the opposite direction requires intersection of the hysteresis loop.

Therefore, we believe that the described characteristics are related to the multistability of the system of dipole-interacting particles. The problem of its transition to the supermagnetic state should be considered based on the temperature dependence of the observed collective effects. Such a dependence is indicated by qualitative changes in the magnetization curve of a sample with a rectangular unit cell induced by a temperature rise to 77 K (see Fig. 4).

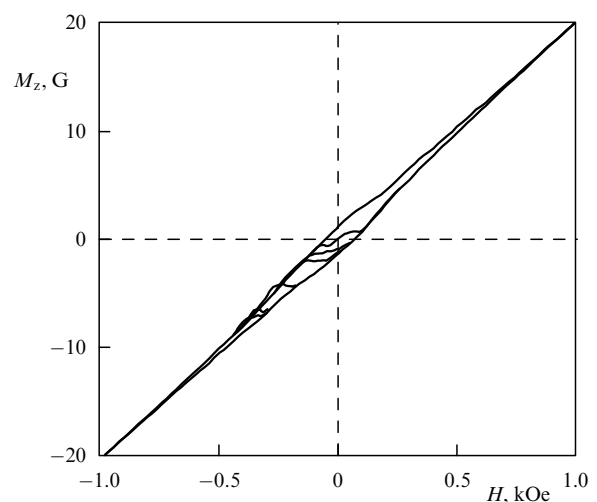


**Figure 4.** Dependence of the sample magnetization on the external magnetic field aligned parallel to the chains ( $\theta = 0$ ). The lower branch corresponds to a field increase from  $-1$  to  $1$  kOe; the upper one, to a decrease from  $1$  to  $-1$  kOe. Transitions from one branch to another result from a change in the sign of the time derivative of the external field.

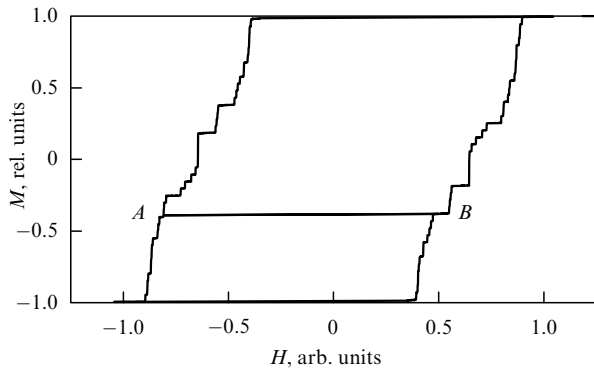


**Figure 5.** Numerical simulation of the magnetization process in a dipole lattice (1:2) consisting of 36 chains of 6 dipoles each; the external magnetic field is applied parallel to the chains. Horizontal line shows one of the feasible transitions between hysteresis branches; *A* and *B* are the states with similar magnetization distributions.

This work was supported by the Russian Foundation for Basic Research (project 98-02-16183) and the Program “Physics of solid-state nanostructures” (project 98-074) of the Russian Ministry of Science and Technology.

## References

1. Simonds J L *Phys. Today* **48** (4) 26 (1995)
2. Rozenbaum V M, Ogenko V M, Chuiko A A *Usp. Fiz. Nauk.* **161** (10) 79 (1991) [*Phys. Usp.* **34** 883 (1991)]
3. Morup S *Europhys. Lett.* **28** (9) 671 (1994)
4. Sugavara A, Sheinfein M R *Phys. Rev. B* **56** (4) R8499 (1997)
5. Gider S et al. *Appl. Phys. Lett.* **69** 3269 (1996)
6. Lok J G S et al. *Phys. Rev. B* **58** 12201 (1998)
7. Bukharaev A A et al. *Fiz. Tverd. Tela* **40** 1277 (1998) [*Phys. Solid State* **40** 1163 (1998)]
8. Gusev S A et al. *Pis'ma Zh. Eksp. Teor. Fiz.* **68** 475 (1998) [*JETP Lett.* **68** 509 (1998)]
9. Usov N A Personal communication
10. Ishii Y, Nakazawa Y *J. Appl. Phys.* **81** 1847 (1996)
11. Gross M, Kiskamp S *Phys. Rev. Lett.* **79** 2566 (1997)
12. Bak P, Bruinsma R *Phys. Rev. Lett.* **49** 249 (1982)

PACS numbers: 73.20.-r, 73.23.-b, 73.40.Gk  
DOI: 10.1070/PU2000v043n03ABEH000701

## Theory of coherent oscillations in a resonant tunneling diode

V F Elesin, I Yu Kateev, A V Krasheninnikov,  
A I Podlivaev

### 1. Introduction

Resonant tunneling and negative differential conductance in a resonant tunneling diode (i.e., in a double-barrier quantum well or quantum dot) are known to be related to the appearance of a resonance level energy due to the spatial quantization phenomenon [1, 2]. Negative differential conductance accounts for the possibility of generating electromagnetic waves. Oscillations in a resonant tunneling diode at a frequency of up to 712 GHz were demonstrated in Refs [3, 4].

However, the extensive application of oscillations based on resonant tunneling diodes is hampered by their relatively low powers and frequencies. What is responsible for such a situation and how a further rise in the power can be achieved

remains unclear, probably because it is intrinsically difficult to give a theoretical description of the resonant tunneling diode. Although there are a relatively large number of theoretical works [4–6] on the subject based primarily on the use of numerical methods, many aspects of the problem need to be elucidated in greater detail, e.g.,

(1) Is there a fundamental limitation on the frequency of oscillations in the resonant tunneling diode? According to a widespread viewpoint [5, 6], the frequency of the resonant tunneling diode is restricted by the resonance level width  $\Gamma$  (or by the inverse characteristic lifetime of an electron in a quantum well,  $\tau_y^{-1} = \Gamma$ ,  $\hbar = 1$ ). This is actually true of ‘classical’ generators, e.g., the Gunn diode.

(2) Is the resonant tunneling diode a ‘quantum’ or a ‘classical’ oscillator, with the properties determined by the parameters of negative differential conduction?

(3) How does the resonant tunneling diode generation power depend on the bias voltage and structure parameters?

The present paper reports selected results recently obtained in an attempt to answer these and other questions.

### 2. Linear theory of the resonant tunneling diode

The studies described in Refs [7, 8] were conducive to the development of the analytical theory of coherent oscillations in the resonant tunneling diode in the approximation linear in the electromagnetic field  $E$ . The coherent regime suggests that the electron’s inverse lifetime in a quantum well  $\tau_y = \Gamma^{-1}$  is shorter than the time of loss of coherence. For the simplest model of a double-barrier structure, an exact solution of the Schrödinger equation with open boundary conditions was found along with active ( $J_c$ ) and reactive ( $J_s$ ) polarization currents which determine the rate of the field increase ( $J_c$ ) and its frequency  $\omega$ .

Using small parameters  $\omega/\varepsilon_R$  and  $\Gamma/\varepsilon_R$  inherent in the resonant tunneling diode ( $\varepsilon_R$  is the resonance level energy), expressions for the polarization currents  $J_c$  and  $J_s$  can be reduced to a simple and clear form:

$$\tilde{J}_c(\omega, \delta) = \frac{4J_c}{e^2 E a Q} = -\frac{\Gamma^2 \delta}{[(\delta + \omega)^2 + \Gamma^2][(\delta - \omega)^2 + \Gamma^2]}, \quad (1)$$

$$\tilde{J}_s(\omega, \delta) = \frac{\Gamma \omega [\delta^2 - \omega^2 - 3\Gamma^2]}{[\delta^2 + \Gamma^2][(\delta + \omega)^2 + \Gamma^2][(\delta - \omega)^2 + \Gamma^2]}. \quad (2)$$

Here,  $\delta = \varepsilon - \varepsilon_R$ ;  $\varepsilon$  is the resonance energy of electrons entering the quantum well from the emitter with a velocity  $Q$  (in our model, the energy  $\varepsilon$  is equivalent to a constant voltage applied to the quantum well); and  $a$  is the quantum well size.

The character of the frequency dependence of the current  $\tilde{J}_c(\omega, \delta)$  is critically related to the ratio  $\delta/\Gamma$ . If  $\delta < \Gamma$ , then the current  $\tilde{J}_c$  has a maximum at  $\omega = 0$  (Fig. 1) and drops with frequency as  $1/\omega^4$ . Near the maximum at  $\omega \ll \Gamma$ , the current  $\tilde{J}_c$  is expressed through the differential conductance of the constant current  $J_0(\delta)$ :

$$\tilde{J}_c = \frac{\partial J_0(\delta)}{\partial \varepsilon}, \quad J_0 = \frac{\Gamma^2}{2(\delta^2 + \Gamma^2)}. \quad (3)$$

The largest increase is achieved at  $\delta = \Gamma/\sqrt{3}$ , where the negative differential conductance has a maximum absolute value. It is  $\delta = \Gamma/\sqrt{3}$  that is normally chosen in both experimental and theoretical studies. In this case, the